IEEE Access
Multidisciplinary | Rapid Review | Open Access Journal

Received 26 January 2024, accepted 12 February 2024, date of publication 26 February 2024, date of current version 6 March 2024.

Digital Object Identifier 10.1109/ACCESS.2024.3369888

RESEARCH ARTICLE

Coexistence of 5G Communication Systems With Radar Altimeters

JIAQI LI, (Member, IEEE), SHUZHI LIU, (Graduate Student Member, IEEE), HOUJIN LU, (Graduate Student Member, IEEE), AND SEUNG-HOON HWANG, (Senior Member, IEEE)

Department of Electronics and Electrical Engineering, Dongguk University, Seoul 04620, South Korea

Corresponding author: Seung-Hoon Hwang (shwang@dongguk.edu)

This work was supported by the Electronics and Telecommunications Research Institute (ETRI) through the ICT Research and Development Program of MSIT/IITP (Development of time–space-based spectrum engineering technologies for the preemptive use of frequencies) under Grant 2017-0-00066.

ABSTRACT With the growing demand for 5G, many countries have allocated additional spectrum above 3.7 GHz, potentially causing serious interference to radar altimeters operating at the 4.2–4.4 GHz band. Therefore, in this paper, a general mathematical model is proposed to estimate interference from 5G base stations to a radar altimeter which can be applied for aircraft, helicopters, unmanned aerial vehicles, satellites, and hot-air balloons. Using this model, the interference at the radar altimeter is evaluated in several environments such as rural, suburban, and urban. Two types of antennas are considered which are omnidirectional and multiple-input and multiple-output antennas (4-by-4, 8-by-8, and 16-by-16). Additionally, a power control-aided distance protection method is introduced to enable the coexistence of the 5G base stations and the radar altimeters. To validate the effectiveness of the proposed protection method, the Monte Carlo method is employed. Numerical results present the heights of the radar altimeter where the interference-to-noise ratio becomes higher than the interference protection threshold of -6 dB. In addition, it shows that the radar altimeter can coexist with the 5G base stations with the proposed protection scheme.

INDEX TERMS Coexistence, 5G base station, radar altimeter, radio interference, 5G, non-terrestrial network, interference analysis, protection, mid-band.

I. INTRODUCTION

C-band (3.4 GHz - 4.2 GHz) has been a strong candidate for the deployment of 5G-cellular systems because the mid-band spectrum has the advantages of wide coverage and high capacity. C-band allocation for 5G services in many countries [1] is shown in Figure 1. Furthermore, for the realisation of the beyond 5G (B5G) and 6G, it is essential to consider the spectrum ranging from low, mid and high bands.

In 2021, the Federal Aviation Administration (FAA) raised the potential interference of 5G with aircraft electronics like radar altimeters (RAs) [3]. Interference from 5G base stations to the RA can result in either missing or incorrect RA information, thus leading to fatal aircraft accidents. Therefore, several international airlines have announced to cancel flights to the United States due to uncertainty about potential interference between new 5G mobile phone services and critical aircraft technology [4]. The RA transmits radio waves to the ground and receives the reflected wave to measure the aircraft's altitude during take-off and landing. The RAs are operated at 4.2 – 4.4 GHz by the spectrum allocation of the International Telecommunication Union (ITU) [5], while the 5G network in the U.S. lies in the range of 3.7 – 3.98 GHz. Since both frequency bands are very close, the FAA raised concerns about the potential interference in the worst case on the safety of the aircraft landing. Besides the U.S., Canada has approved 5G in the C-band with the restrictions of not using the C-band in the vicinity of airports to ensure aviation safety [6]. Additionally, the frequency band of 3.7-4.0 GHz is expected to be reallocated for 5G cellular services in Korea in

The associate editor coordinating the review of this manuscript and approving it for publication was Miguel López-Benítez.

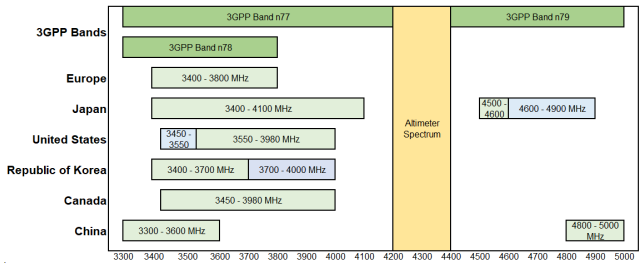

FIGURE 1. 3GPP and mid-band spectrum with the radar altimeter band [2].

TABLE 1. A comparison with the related works.

Ref	Interference	Protection Method
[8]	5G BS → FSS ES	-
[9]	5G BS → FSS ES	√
[10]	5G BS → FSS ES	√
[11]	RA → LTE UE	-
[12]	5G BS/UE → RA	-
[13]	5G BS → RA	-
This Work	5G BS → RA	√

the near future [7]. Therefore, it is very important to evaluate the potential interference from the 5G systems to the RA and investigate the interference reduction schemes to enable their coexistence.

Recent studies on the coexistence of 5G ground-based systems with non-terrestrial networks have mainly focused on satellite earth stations (ES). However, there has been a lack of focus on RAs. Reference [8] formulated an interference analysis modelling to assess the coexistence of IMT-2020 and existing satellite services in the mmWave band, considering the factors such as propagation loss, antenna arrays, and multi-scenarios. Reference [9] presented a system model to evaluate the coexistence of FSS ES receivers with 5G cellular downlink and uplink in the C-band, and demonstrated how the interference can be mitigated by deactivating base stations located close to the FSS ES receiver. Reference [10] addressed the same interference issues and proposed a solution for the coexistence of the ES and 5G base stations based on the distance protection method in such scenarios as RMa, UMa, and UMi. Also, the exclusion and the restriction zones were defined based on elevation angles. However, [8], [9], and [10] did not consider the RA.

The work of [11] proposed an analysis method to evaluate the impact of interference from RAs on long-term evolution (LTE) user equipments (UE) when RAs share the 4.2 – 4.4 GHz band with LTE. However, the study did not provide conclusive findings on the feasibility of this sharing. In a joint report of the FAA and the Radio Technical Commission for Aeronautics [12], the interference analysis methodology and the RA interference tolerance threshold were considered. The report indicated that RAs receive harmful interference from 5G base stations. Another study [13] performed the interference analysis between the 5G system and the RA based on the Monte Carlo method when the aircraft was at 100 m and 200 m in the suburban environment. However, the in-depth description was not included in these studies such as antenna types and the loss models without any interference reduction methods. S. Futatsumori et al. developed a measurement method for the interference path loss at the RA and discussed the possibilities of the spectrum sharing between the wireless avionics intra-communication (WAIC) systems and the RAs [14], [15]. In [16], the interference of 5G signals ranging from 0 to 1,500 ft was evaluated with the criteria of pulsed RA in 5G systems, which describes that the interference power threshold decreases as the altitude increases. Table 1 summarises the comparisons with the related studies.

Drones, also known as unmanned aerial vehicles (UAVs), may experience a similar problem since they are expected to be integrated into B5G and 6G multi-layer network architecture [17]. The study in [18] explored the impact on the performance of ground-based UE with cellular-connected drones. Additionally, the studies in [19] and [20] examine interferences from the noise beam of the ground base stations to the UAV, resulting in frequent handovers.

To analyse the interference from 5G base stations on flying objects, a mathematical method to calculate the interference power received by the RA was proposed in our previous study of [21], which first calculated the interference power from a 5G base station and then multiplied it by the number of 5G base stations within the coverage of the RA, i.e., 3 dB beamwidth of the RA. Therefore, this paper extends the interference calculation model presented in [21] by describing the 5G base station gain and the path loss in more details. Also, the interference is analyzed based on the model. To reduce the interference for the coexistence, a new power control-aided distance protection scheme is proposed. Finally, the feasibility of the proposed scheme is confirmed by the Monte Carlo method. The main contributions of this work can be summarised as follows:

- An interference calculation model has been built up to calculate the interference from the ground-based base stations on the flying objects, which is applicable for aircraft, helicopters, UAVs, and hot-air balloons.
- A power control-aided distance protection method has been used to enable the coexistence of 5G base stations and the RA.
- The proposed protection method has been validated by the Monte Carlo simulation.

The remainder of this paper is organized as follows. Section II describes the interference power calculation. Section III describes the interference analysis between the 5G base station and the RA. Section IV presents the power control-aided distance protection method. Section V focuses on validating whether the protection method may permit the coexistence with the RAs and the 5G system. Finally, we conclude the contributions of this paper in Section VI.

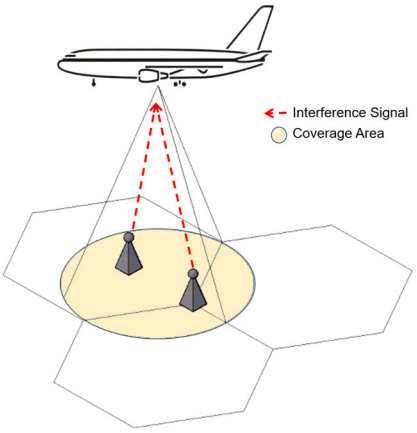

FIGURE 2. The interference scenario where the radar altimeter receives Interference signal power from the 5G base stations.

II. INTERFERENCE POWER CALCULATION

In this section, an interference analysis model is developed to calculate the total interference signal power in the interference scenario of Figure 2. Firstly, the single interference power generated from a 5G base station is calculated as follows:

$$I_{single,i} = P_{t,i} + G_{BS,i} + G_{RA} - PL_i - L_{cable} - L_{polar,i} - L_{body,i} - OTR \quad (1)$$

where $P_{t,i}$ and $G_{BS,i}$ are the transmitted power and antenna gain of the i^{th} 5G base station, respectively. G_{RA} is the antenna gain of the RA and OTR is the on-tune rejection. PL_i, L_{cable}, $L_{polar,i}$, and $L_{body,i}$ are the path loss, cable loss, polarization loss, and body loss, respectively.

The radius of the coverage area is expressed as follows [22].

$$R_{RA} = h_{RA} \cdot tan\left(\frac{\emptyset_{3dB}}{2}\right) \quad (2)$$

where h_{RA} is the current RA height and $\emptyset_{3dB}$ is the 3dB beamwidth of the RA antenna. The number of the 5G base stations in the coverage area is approximated using the following equation:

$$N_{BS} = \left\lceil \left(\frac{R_{RA}}{R_{BS}}\right)^2 \right\rceil \quad (3)$$

where R_{BS} is the cell radius of the base station. Therefore, the total interference signal power received by the RA is the aggregate of all 5G base stations as follows:

$$I = 10log_{10}\left(\sum_{i=1}^{N_{BS}} 10^{\frac{I_{single,i}}{10}}\right) \quad (4)$$

Also, N is the effective thermal noise of the RA and is calculated by

$$N = -114 + 10log_{10}(BW_{RA}) + N_F \quad (5)$$

where BW_{RA} is the channel bandwidth of the RA and N_F is the noise figure. Using Equations. (4) and (5), the interference-to-noise ratio (I/N) may be calculated and compared with the interference protection criteria value in Report ITU-R M.2059-0.

A. ANTENNA GAIN OF A BASE STATION BEAMFORMING

The directivity of the multi-input, multi-output (MIMO) antenna is achieved by increasing the number of arrays to compress the beamwidth. Therefore, the antenna gain of the base station beamforming involves the antenna element gain and the beamforming gain [23]. The single-element pattern can be represented by the sum of two components.

The single-element pattern in the horizontal range is expressed as

$$A_H(\varphi) = -min\left[12\left(\frac{\varphi}{\varphi_{3dB}}\right)^2, A_m\right] \quad (6)$$

The single-element pattern in the vertical range is expressed as

$$A_V(\varphi) = -min\left[12\left(\frac{\theta - 90}{\theta_{3dB}}\right)^2, SLA_V\right] \quad (7)$$

Therefore, the single-element pattern is given by

$$A_E(\varphi, \theta) = G_{E,max} - min\{-[A_H(\varphi) + A_V(\varphi)], A_m\} \quad (8)$$

where φ_{3dB} and θ_{3dB} are the horizontal and vertical 3dB bandwidths of an element, respectively. Both A_m and SLA_V are the front-to-back ratios, and $G_{E,max}$ is the element gain. The elevation and azimuth angle of the signal direction are denoted by θ and φ, respectively.

The beamforming array gain is calculated by

$$A_{array} = 10log_{10}\left(\left|\sum_{m=1}^{N_H}\sum_{n=1}^{N_V} w_{n,m} \cdot v_{n,m}\right|^2\right) \quad (9)$$

where N_V and N_H are the number of elements in the rows and columns of the antenna array, respectively. $v_{n,m}$ is the super position vector represented by

$$v_{n,m} = exp\left\{\sqrt{-1} \cdot 2\pi\left[(n-1)\frac{d_V}{\lambda} \cdot cos(\theta) + (m-1)\frac{d_H}{\lambda} \cdot sin(\theta) \cdot sin(\varphi)\right]\right\} \quad \forall n \in [1 \cdots N_V], m \in [1 \cdots N_H] \quad (10)$$

$w_{n,m}$ is the weighting of the beamforming represented by

$$w_{n,m} = \frac{1}{\sqrt{N_V \cdot N_H}} exp\left\{\sqrt{-1} \cdot 2\pi\left[(n-1)\frac{d_V}{\lambda}\right] \cdot sin(\theta_{etilt}) - (m-1)\frac{d_H}{\lambda} \cdot cos(\theta_{etilt}) \cdot sin(\varphi_{escan})\right\} \quad (11)$$

where $\frac{d_V}{\lambda}$ and $\frac{d_H}{\lambda}$ are the vertical and horizontal radiating element spacing, respectively; θ_{etilt} is the mechanical downtilt angle; and φ_{escan} is the wide-scan angle.

In short, the beamforming antenna gain of a 5G base station is expressed by

$$G_{BS} = A_E(\varphi, \theta) + A_{array} \quad (12)$$

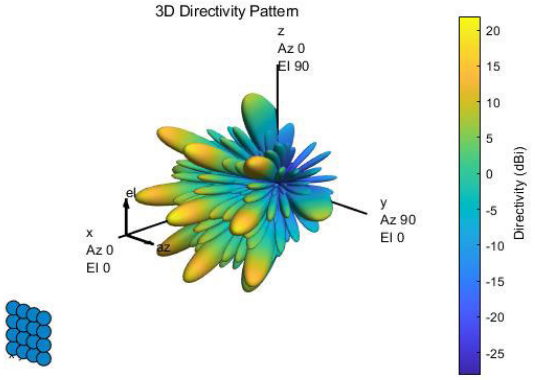

(a) 4-by-4

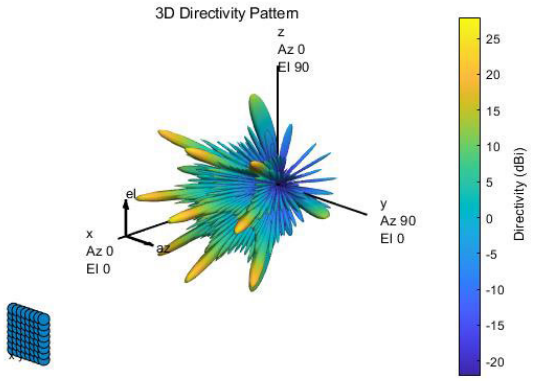

(b) 8-by-8

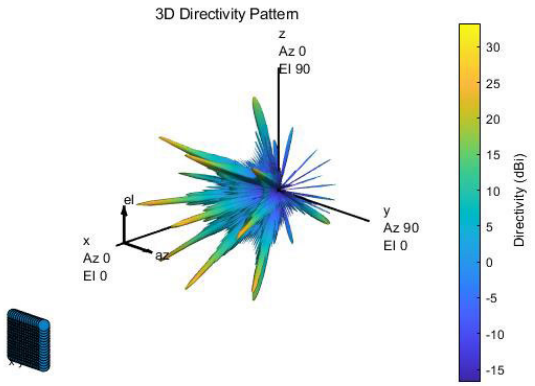

(c) 16-by-16

FIGURE 3. Three-dimensional array beam patterns.

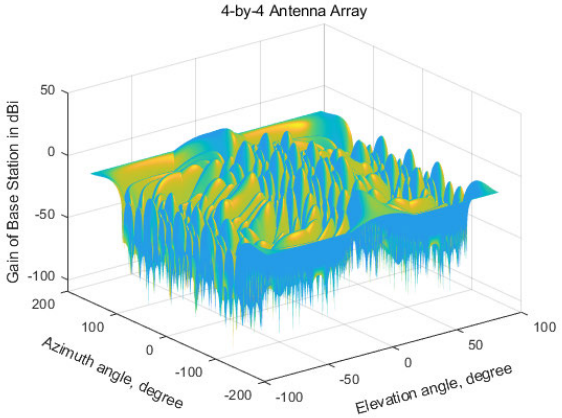

(a) 4-by-4

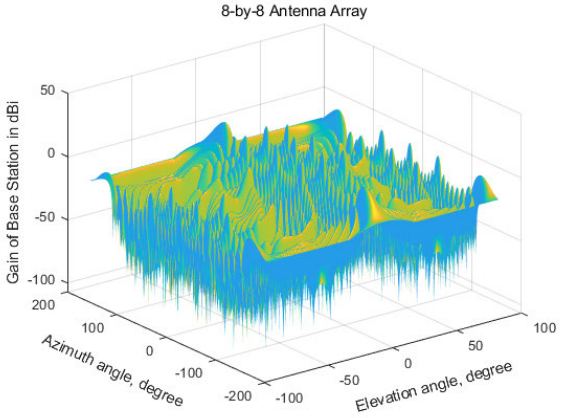

(b) 8-by-8

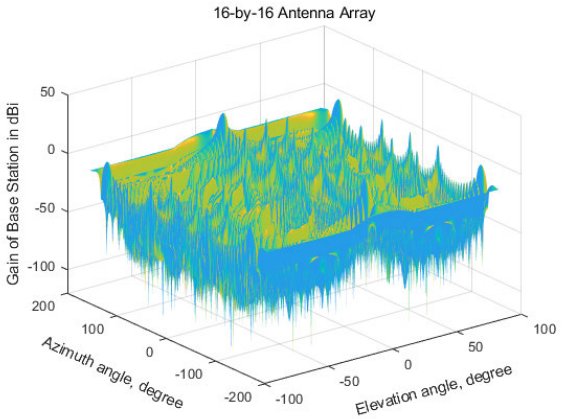

(c) 16-by-16

FIGURE 4. Antenna gain of the 5G base station.

The drawback using a C-band is to increase atmospheric attenuation such as free space loss or rainfall attenuation [24]. To overcome the drawback, a lot of antenna elements in the array are employed to achieve beamforming gain and enhance the directivity. In this study, we employ MIMO with 4-by-4, 8-by-8, and 16-by-16 antenna arrays. The three-dimensional beam patterns are shown in Figure 3, which demonstrates that the beamwidth becomes significantly narrower and the side-lobes' amplitude smaller, as the number of antenna elements increase.

Additionally, the antenna gain in terms of azimuth and elevation angles is investigated in Figure 4. The azimuth angle is plotted on the x-axis ranging from -180 to 180 degrees. Meanwhile the elevation angle is displayed on the y-axis ranging from -90 to 90 degrees. The results show that a higher antenna directivity and a larger gain in the main beam direction are obtained with an increase of the number of antenna elements. For example, the maximum gains for the 4-by-4, 8-by-8, and 16-by-16 antenna arrays are measured as 18.4412 dBi, 24.4618 dBi, and 30.4824 dBi, respectively.

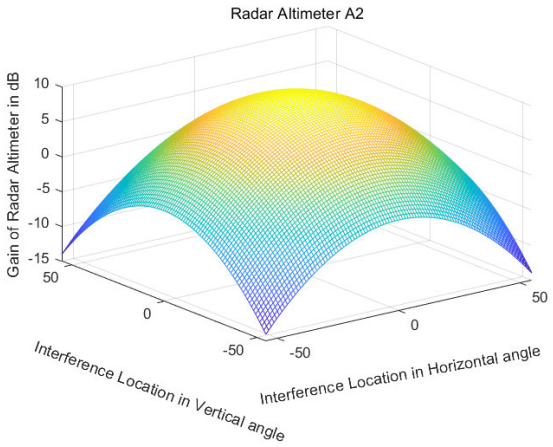

FIGURE 5. Antenna gain of the radar altimeter A2.

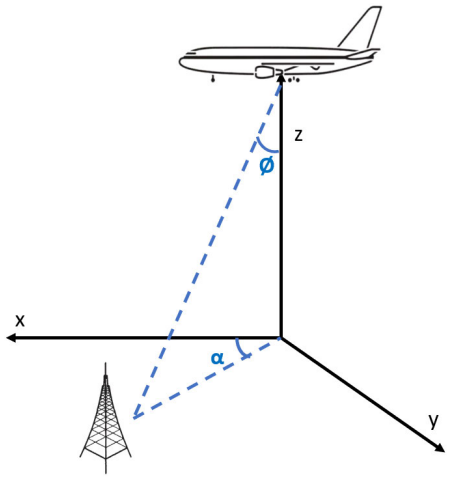

FIGURE 6. The three-dimensional cartesian coordinate system of the interference scenario.

B. ANTENNA GAIN OF THE RA

The gain of a RA is given by [25]

$$G_{RA}(\emptyset) = -\frac{12}{\emptyset_{3dB}^2}\emptyset^2 + G_{RA,max} \tag{13}$$

where $G_{RA,max}$ is the maximum RA antenna gain; $\emptyset_{3dB}$ is the 3dB beamwidth of the RA antenna; and $\emptyset$ is the incident angle measured from the altimeter bore site. In this study, the parameters of the RA A2 defined in Rec. ITU-R M.2059-0 are used for the simulation. Figure 5 depicts the gain of the RA according to the location of the 5G base station, where the gain of the RA reaches maximum when the 5G base station is directly below the RA, because the incident angle is precisely 0 degrees.

C. LOCATION DEFINITION

The location of the 5G base station with coordinate (x_{BS}, y_{BS}, h_{BS}) is determined by a three-dimensional cartesian coordinate system. The position of the RA is always defined along the z-axis with coordinates (0, 0, h_{RA}). The three-dimensional cartesian coordinate system of the interference scenario is illustrated in Figure 6.

$$x_{BS} = cos(\alpha) \cdot tan(\emptyset) \cdot h_{RA} \tag{14}$$

$$y_{BS} = sin(\alpha) \cdot tan(\emptyset) \cdot h_{RA} \tag{15}$$

The angles α and $\emptyset$ were determined by two random variables x_1 and x_2 with uniform distribution between 0 and 1.

$$\alpha = 2\pi \cdot x_1 \tag{16}$$

$$\emptyset = \frac{\emptyset_{3dB}}{2} \cdot x_2 \tag{17}$$

The range of the incident angle $\emptyset$ of the RA changes with a change in the altimeter height which is given by

$$\emptyset \in \left[-\frac{\emptyset_{3dB}}{2}, \frac{\emptyset_{3dB}}{2}\right] \tag{18}$$

Consequently, the distance between the base station and the RA was calculated as follows:

$$d = \sqrt{x_{BS}^2 + y_{BS}^2 + (h_{BS} - h_{RA})^2} \tag{19}$$

D. PATH LOSS

The calculations of path loss in rural, suburban and urban scenarios are represented in [26]. The path loss for line-of-sight (LOS) channels in the rural scenario is expressed as

$$PL_{LOS} = 33.51 + 20log_{10}(\pi d) + 0.49 \cdot log_{10}(d) - + 0.0014 \cdot d \tag{20}$$

Also, the path loss for non-line-of-sight (NLOS) channels in the rural scenario is formulated as

$$PL_{NLOS} = max\left(PL_{LOS}, 15.31 + 38.63 \cdot log_{10}(d)\right) \tag{21}$$

In the suburban scenario, the path loss for LOS channels is expressed as

$$PL_{LOS} = 39.71 + 22log_{10}(d) \tag{22}$$

while the path loss for the NLOS channels is expressed as

$$PL_{NLOS} = max\left(PL_{LOS}, 25.25 + 39.08 \cdot log_{10}(d)\right) \tag{23}$$

In the urban scenario, the path loss for LOS channels is expressed as

$$PL_{LOS} = 44.11 + 21log_{10}(d) \tag{24}$$

For the NLOS channels, the path loss is expressed as

$$PL_{NLOS} = max\left(PL_{LOS}, 34.87 + 35.3 \cdot log_{10}(d)\right) \tag{25}$$

Figure 7 depicts the path loss of the RA ranging from 50 to 1,500 ft in rural, suburban, and urban [15], [33]. Note that the 5G base station is assumed to be located directly below the RA for arbitrary RA height. The results reveal that the lowest path loss appears at 115 ft (35.05 m), 82.5 ft (25.146 m), and 65 ft (19.812 m) in the rural, suburban, and urban scenarios, respectively. Note that the path loss curves for LOS and NLOS conditions are perfectly matched in the rural scenario. It means that signal attenuation is relatively less affected in the rural scenario because of its expansive

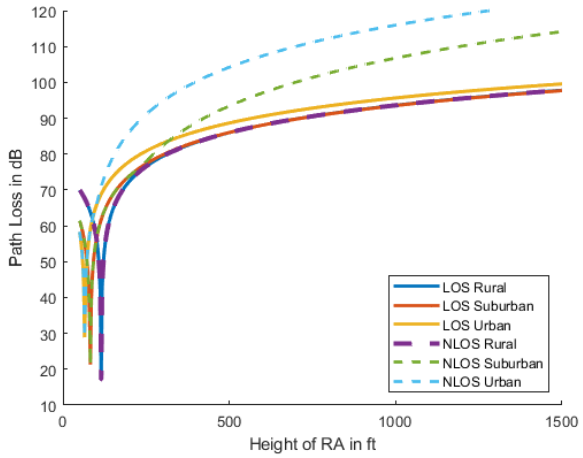

FIGURE 7. Path loss vs. the height of the RA in rural, suburban and urban scenarios.

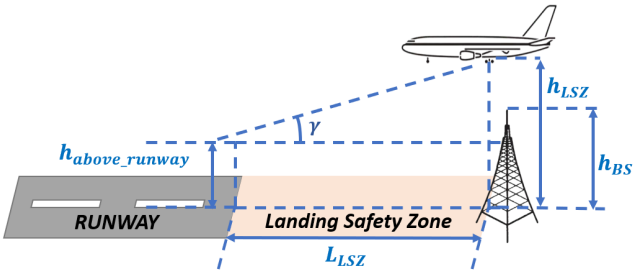

FIGURE 8. Landing scenario with landing safety zone.

open spaces and farmlands [38]. In the suburban scenario, the LOS and NLOS path loss curves are overlapped when the height of the RA is below 235 ft. This indicates that within this altitude range, the attenuation is consistent for both LOS and NLOS channels. In the urban scenario, the LOS and NLOS path loss curves similarly overlap below 100 ft of the RA height. However, over the certain radio altimeter height, the path loss is significantly diverged.

E. ON-TUNE REJECTION

On-tune rejection (OTR) is the rejection of an undesired co-tune signal which is a factor for on-channel impact. The OTR is defined [27] in dB as follows:

$$OTR = \begin{cases} 0, for BW_{tx} \leq BW_{rx} \\ 20log_{10}\left(\dfrac{BW_{tx}}{BW_{rx}}\right), for BW_{tx} \geq BW_{rx} \end{cases} \quad (26)$$

where BW_{tx} and BW_{rx} are the transmitter and receiver channel bandwidths, respectively.

III. INTERFERENCE ANALYSIS BETWEEN THE 5G BASE STATION AND THE RA

In this section, using the mathematical model in Section II, the interference analysis is performed with the existing RA services at the 4.2–4.4 GHz band and the 5G system at the 3.7–4.0 GHz band. Considering the realistic landing scenario, a landing safety zone and a zero-interference zone are introduced and described. Then, the interference will be analyzed.

TABLE 2. Landing safety zone and relative airplane height.

Scenario	L_{LSZ} (Unit: m)	h_{LSZ} (Unit: ft)
Rural	93.75	133
Suburban	56.40	100
Urban	40.40	86

A. LANDING SAFETY ZONE

To ensure the safety of aircraft during take-off or landing, the surroundings of runway such as artificial buildings or trees must be limited in height [28]. Therefore, any 5G base station cannot be deployed around the runway when the airplane height becomes below the base station height. Figure 8 shows a landing scenario with landing safety zone (L_{LSZ}) where an angle of γ ranging from 10 to 15 degrees as the landing downward angle determines the landing safety zone before the runway [30]. The airplane is assumed to arrive at the middle of the runway, which employs γ as 15 degrees [31].

The length of L_{LSZ} can be obtained by

$$L_{LSZ} = \frac{h_{BS} - h_{above\_runway}}{tan(\gamma)} + \frac{1}{2}L_{fuselage} \quad (27)$$

where h_{BS} is the antenna height of the 5G base station, h_{above_runway} is the minimum altitude of an airplane above the edge of the runway, and γ is the landing downward angle. The base station antenna height is 35 m in the rural, 25 m in the suburban, and 20 m in the urban environment [32]. Assuming that the RA is mounted at the center of the airplane's bottom, the half the length of the fuselage ($L_{fuselage}$) is additionally considered in the landing safety zone. The data for a Boeing 737-800 is used, which indicates the fuselage length is 39.5 m [29]. The relative airplane height (h_{LSZ}) indicates the airplane height at the point where the airplane starts to enter the landing safety zone by

$$h_{LSZ} = tan(\gamma) \cdot L_{LSZ} + h_{above\_runway} \quad (28)$$

Using Equations (23) and (24), the specific values are summarized in Table 2.

When the airplane starts entering the landing safety zone, the RA height, h_{RA}, is less than or equal to the relative height of the landing safety zone, h_{LSZ}. Therefore, $\emptyset$ is expressed as follows:

$$\emptyset \in \left[\frac{\emptyset_{3dB}}{2} - arctan\left(\frac{L_{LSZ}}{h_{RA} - h_{above\_runway}} - \frac{1}{tan(\gamma)}\right), \frac{\emptyset_{3dB}}{2}\right] \quad (29)$$

B. ZERO-INTERFERENCE ZONE

As an aircraft enters the landing safety zone, the RA can still receive interference signals because of the RA coverage. Therefore, we define zero-interference zone which is calculated as follows:

$$L_{zero} = \frac{L_{LSZ}}{tan\left(\frac{\emptyset_{3dB}}{2}\right) \cdot tan(\gamma)} \quad (30)$$

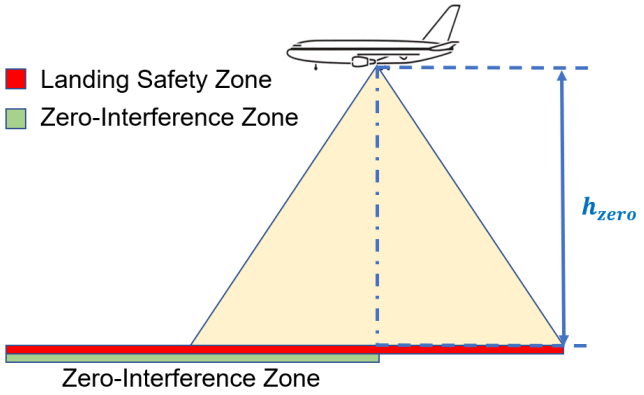

FIGURE 9. Definition of the zero-interference zone.

Algorithm 1 Pseudo-code to Obtain the Zero-Interference Zone

Require: Identify the length of the landing safety zone (L_{LSZ}) and its relative radar altimeter height (h_{LSZ})

1: **for** each radar altimeter height (h_{RA}) **do**
2: **if** $h_{RA} \leq h_{LSZ}$ **then**
3: Calculate the approaching distance ($d_{approaching}$)
4: Calculate the radius of the radar altimeter (R_{RA})
5: $d \leftarrow d_{approaching} + R_{RA}$
6: **if** $d \leq h_{LSZ}$ **then**
7: Storage $d_{approaching}$ in the list of the zero-interference zone
8: Calculate the relative height of the radar altimeter as h_{zero}
9: **else**
10: $h_{RA} \leftarrow h_{RA} + 1$
11: Go back to the beginning of the for section
12: **end if**
13: **else**
14: $h_{RA} \leftarrow h_{RA} + 1$
15: Go back to the beginning of the **for** section
16: **end if**
17: **end for**

TABLE 3. Zero-Interference zone and relative airplane height.

Scenario	Zero-Interference Zone [L_{zero}] (Unit: m)	Corresponding Height [h_{zero}] (Unit: ft)
Rural	93.48	116
Suburban	55.89	87
Urban	40.34	75

The flowchart shown in Algorithm 1 illustrates how to obtain the length of the zero-interference zone (L_{zero}) and the corresponding altimeter height (h_{zero}). As the airplane descends below h_{zero}, there is no interference from the 5G base stations. h_{zero} depends not only on the landing safety zone but also the beamwidth of the RA. Since the 3 dB beamwidth of the A2 RA is 55 degrees in [3], the zero-interference zone and its corresponding height are calculated in Table 3.

C. ANALYSIS OF INTERFERENCE BETWEEN THE 5G BASE STATIONS AND THE RA

For the interference analysis, the worst-case may be assumed the maximum transmitted power of the 5G base stations, the maximum antenna gains of the base stations and the RA, and the base station deployment right below the RA. Also, all channels are assumed to be LOS channels. The 5G base station is modeled with the parameters in Table 4. The parameters for the RA are mentioned in Table 5.

Figure 10 represents the simulation results for the received interference from the base stations when the RA height is

TABLE 4. 5G base stations parameters.

Parameters [Symbol]	Unit	Value
Maximum transmitted power [$P_{t,max}$]	dBm	Rural: 71 Suburban, Urban: 68
Minimum transmitted power [$P_{t,min}$]	dBm	24 [34]
Transmitter bandwidth [BW_{tx}]	MHz	100
Receiver bandwidth [BW_{rx}]	MHz	20
Antenna height [h_{BS}]	m	Rural: 35 Suburban: 25 Urban: 20
Cell radius [R_{BS}]	m	Rural: 1200 Suburban: 600 Urban: 300
Base station gain [G_{BS}]	dB	Omnidirectional: 18
Element gain in MIMO [$G_{E,max}$]	dB	6.4
UE antenna height [h_{UE}]	m	1.5
Front-to-back ratio [A_m, SLA_V]	dB	30
Building height [h]	m	5
Elevation angle [θ]	°	[-90, 90]
Azimuth angle [φ]	°	[-180, 180]
Horizontal 3dB beamwidth [φ_{3dB}]	°	90
Vertical 3dB beamwidth [θ_{3dB}]	°	65
Horizontal element spacing [$\frac{d_H}{\lambda}$]		0.5λ
Vertical subarray spacing [$\frac{d_V}{\lambda}$]		2.1λ
Base station antenna array [$N_V \times N_H$]		4×4, 8×8 and 16×16
UE antenna array [$N_V \times N_H$]		2×2
Carrier frequency	GHz	3.7 – 4.0
Central frequency [f_c]	GHz	3.85
Duplex		TDD
Polarization	°	45
Mechanical downtilt angle [θ_{etilt}]	°	Rural: 3 Suburban: 6 Urban: 10
Modulation		QPSK [35]
Noise temperature [T]	K	290
Body loss [L_{body}]	dB	4
Polarization loss [L_{polar}]	dB	3

TABLE 5. Radar altimeter parameters.

Parameters [Symbol]	Unit	Value
Nominal center frequency	GHz	4.3
Carrier frequency	GHz	4.2 – 4.4
Channel bandwidth	MHz	196 [36]
Radar altimeter height [h_{RA}]	ft	[50, 1500]
Maximum antenna gain [$G_{RA,max}$]	dB	10
Noise figure [N_F]	dB	6
Cable loss [L_{cable}]	dB	6
3 dB beamwidth [$\emptyset_{3dB}$]	°	55
Modulation		FMCW
Interference protection threshold [$\frac{I}{N_{th}}$]	dB	-6
Noise temperature [T]	K	290
Average landing speed	m/s	74.588 [37]
Fuselage length [$L_{fuselage}$]	m	39.5
Landing downward angle [γ]	°	15

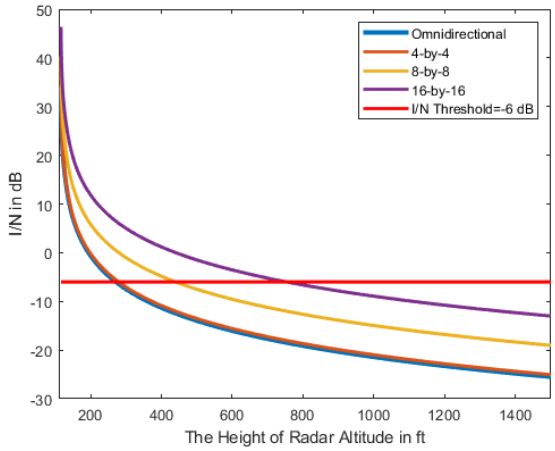

(a) 4-by-4

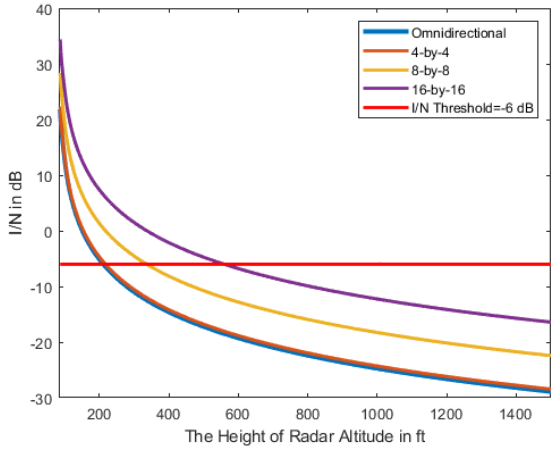

(b) 8-by-8

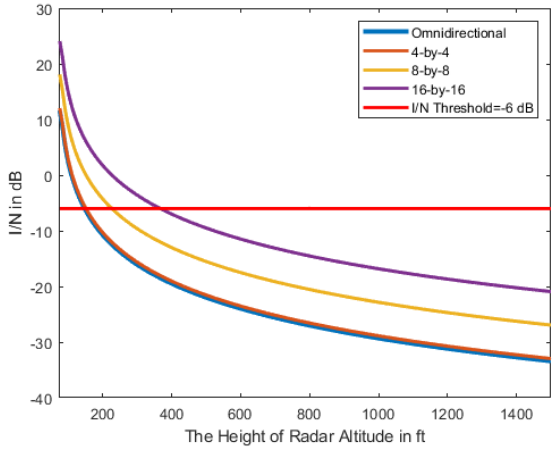

(c) 16-by-16

FIGURE 10. Received interference signal strength vs. the height of radar altimeter.

ranging from h_{zero} to 1,500 ft in the rural, suburban, and urban scenarios. It shows that the interferences increase as the RA height decreases, and then reach the maximum value at h_{zero}. The observation regarding the received interference power among scenarios are as follows: the rural scenario exhibited the highest interference, followed by the suburban scenario, and then the urban scenario with the lowest interference. The tendency is consistent with the path loss behavior. Note that the received interference power is well matched between the omnidirectional antenna and the 4-by-4 antenna array. This is because the peak base station gain of 18 dB for the omnidirectional antenna is almost same with that of 18.4412 dB for the 4-by-4 antenna array.

TABLE 6. The height with I/N over interference protection threshold.

Scenario	Antenna Array	Height [h_{RZ}] (Unit: ft)
Rural	Omnidirectional	271
	4-by-4	279
	8-by-8	439
	16-by-16	753
Suburban	Omnidirectional	211
	4-by-4	217
	8-by-8	336
	16-by-16	559
Urban	Omnidirectional	148
	4-by-4	151
	8-by-8	226
	16-by-16	367

Specifically, in the rural scenario, the received interference-to-noise ratio approaches the threshold of -6 dB as the airplane altitudes is changing: 271 ft for the omnidirectional, 279 ft for 4-by-4, 439 ft for 8-by-8, and 753 ft for 16-by-16 antenna arrays, respectively. When the airplane altitude keeps higher than these heights, the RA never encounters harmful interference from the 5G base stations. Additionally, for $h_{zero} = 116$ ft, the maximum interference-to-noise ratio reaches 33.9034 dB with omnidirectional, 34.3446 dB with 4-by-4, 40.3652 dB with 8-by-8, and 46.3858 dB with 16-by-16, respectively. Comparatively, in the suburban scenario, the height becomes lower than that of the rural case. Specifically, the airplane altitudes are 211 ft, 217 ft, 336 ft, and 559 ft. The received interference reaches the maximum values of 21.9136 dB, 22.3548 dB, 28.3754 dB, and 34.396 dB at 87 ft. In the urban scenario, the heights are 148 ft, 151 ft, 226 ft, and 367 ft for the omnidirectional, 4-by-4, 8-by-8, and 16-by-16 antenna arrays, respectively. It demonstrates that the heights are much lower than the other scenarios due to the higher path loss. The maximum interference power is 11.6221 dB, 12.0633 dB, 18.0839 dB, and 23.6751 dB at 75 ft. A summary of these altitudes in three scenarios can be found for different antenna array in Table 6.

IV. POWER CONTROL-AIDED DISTANCE PROTECTION

To mitigate harmful interference, an effective method is to guarantee geographical separation between the 5G base stations and the RAs. In this approach, the 5G base stations are strategically deployed at a certain distance from the RA in approaching aircraft. Unfortunately, the separation distance results in the reduction of the 5G service area. Therefore, a straightforward approach to diminish separation distance is to reduce the transmitted power of the 5G base stations. In this work, a power control-aided distance protection method is

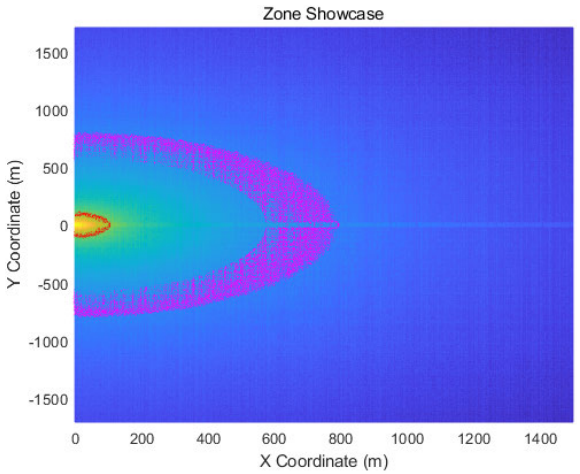

FIGURE 11. Exclusion and restriction zones in the rural scenario with the 16-by-16 antenna array.

proposed to enable the coexistence of the 5G base stations and RAs.

A. PROPOSED POWER CONTROL-AIDED DISTANCE PROTECTION METHOD

There are two different types of zones that are defined in the proposed power control-aided distance protection, i.e., the exclusion and restriction zones. An exclusion zone is an area where any 5G base stations are not allowed to deploy around the airplane's approaching route. It depends on the interference-to-noise ratio after power control, the landing downward angle of the aircraft, and the radius of the RA coverage. The length of the exclusion zone should be set to the horizontal distance between the runway edge and the RA, when the interference is larger than the threshold value even if the power control is applied. Note that the length of the exclusion zone needs to be compared with that of the landing safety zone, in order to define the exclusion zone. On the other hand, a restriction zone is defined as a designated area outside the exclusion zone, where the deployment of 5G base stations is permitted. Note that there is the limitation for the maximum transmit power at the base station. Figure 11 illustrates the example of exclusion and restriction zones in the rural scenario with 16-by-16 antenna array. It indicates the reference point (0, 0) as the center of the runway edge, the red line as the exclusion zone, and the pink line as the restriction zone.

We assume that the transmission power is greater than or equal to the minimum value, even with the power control. The pseudo-code for the power control-aided distance protection algorithm is shown in Algorithm 2. The algorithm starts by calculating the aggregate received interference at the RA for the worst case, which includes several parameters such as the maximum transmitted power from the 5G base stations, the maximum antenna gains for the 5G base stations and the RA, and the path loss in LOS conditions at each RA height. Then, it checks whether the received interference exceeds the threshold or not: if the answer is 'false', then the total received interference and the maximum transmitted power are separately stored in the database. Unless the answer is 'false', then the transmitted power decreases by 0.1 dB for each calculation during the total interference within the threshold or the minimum transmitted power. Once the total received interference falls below the threshold, the current RA height is recorded, and the restriction zone is determined. When the transmitted power is reduced to the minimum transmitted power, and the received interference still exceeds the threshold, the current RA height is stored and then the exclusion zone is decided. Note that the exclusion zone may not exist for all cases.

Algorithm 2 Pseudo-code for Power Control-aided Distance Protection

Require: Initial the scenario parameters
1: **for** each radar altimeter height (h_{RA}) **do**
2: Input the maximum transmitted power ($P_{t,max}$)
3: Input the cable loss (L_{cable})
4: Input the polarization loss (L_{polar})
5: Input the body loss (L_{body})
6: Calculate the maximum base station gain (G_{BS})
7: Calculate the maximum radar altimeter gain (G_{RA})
8: Calculate the path loss (PL) in the LOS condition
9: Calculate the aggregate recevied interference ($\frac{I}{N}_{total}$)
10: **if** $\frac{I}{N}_{total} \leq \frac{I}{N}_{th}$ **then**
11: Store the recevied interference in the list of $\frac{I}{N}$
12: Store the current transmitted power in the list of P_t
13: **else**
14: **for** each step in $P_{t,min} \leq P_t < P_{t,max}$ **do**
15: $P_t \leftarrow P_t - 0.1$
16: Calculate the aggregate received interference ($\frac{I}{N}_{total}$)
17: **if** $\frac{I}{N}_{total} \leq \frac{I}{N}_{th}$ **then**
18: Store the recevied interference in the list of $\frac{I}{N}$
19: Store the current transmitted power in the list of P'_t
20: Store the current radar altimeter height of h_{RA}
21: Obtain the restrcition zone (Z_{RZ})
22: Go back to the first **for** section in line 1
23: **else**
24: **if** $P_t = P_{t,min}$ **and** $\frac{I}{N}_{total} > \frac{I}{N}_{th}$ **then**
25: Store the received interference in the list of $\frac{I}{N}$
26: Store the current radar altimeter height of h_{RA}
27: Obtain the exclusion zone (Z_{EX})
28: **else**
29: **Continue**
30: **end if**
31: **end if**
32: **end for**
33: **end if**
34: **end for**

B. I/N EVALUATION WITH POWER CONTROL

In this section, we analyze the interference with the power control scheme. For the evaluation, the center frequency is assumed to be 3.85 GHz, and the center frequency of RA is 4.3 GHz with the bandwidth of 196 MHz. In addition, the airplane is assumed to be a Boeing 737-800 for the simulation. The height of the RA ranging from h_{zero} to 1,500 ft is considered in rural, suburban, and urban scenarios. In each scenario, four types of antennas are assumed such as the

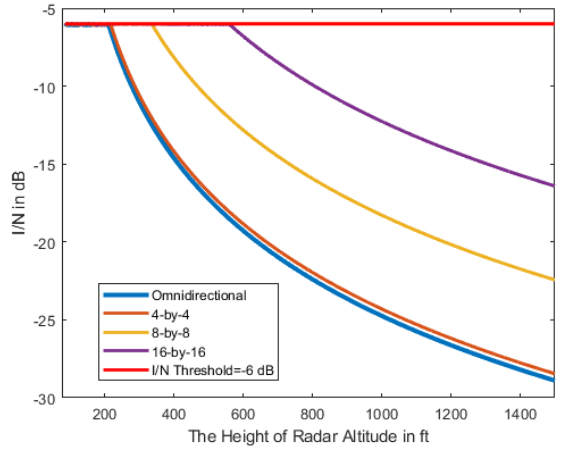

(a) Suburban

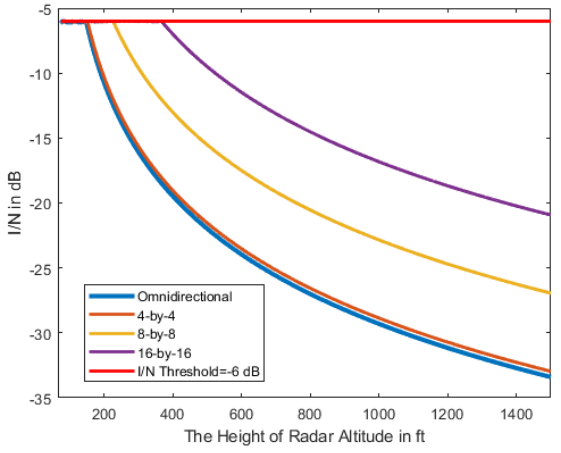

(b) Urban

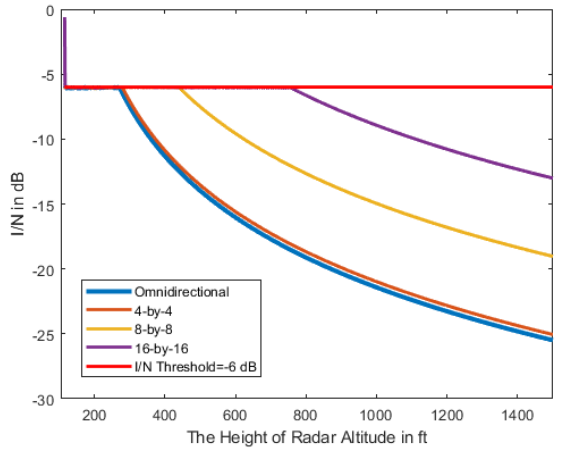

(c) Rural

FIGURE 12. Power-controlled interference-to-noise ratio for various types of antennas under multiple scenarios.

omnidirectional, the 4-by-4, 8-by-8, and 16-by-16 antenna arrays to estimate the interference signal power received by the RAs.

In Figure 12 (a) and (b), the received interference signals in the suburban and urban scenarios are below the interference protection threshold of the RA after the power control algorithm applied. It indicates that the area in the exclusion zone is smaller than the landing safety zone, which describes that the exclusion zone is not needed. The most significant reduction in transmitted power from the 5G base station is observed in the rural scenario, as depicted in Figure 12 (c). A consistent trend is observed except 16-by-16 antenna arrays, mirroring the patterns seen in the suburban and urban scenarios. Upon implementing the power control scheme, the received interference signals are effectively controlled within the prescribed protection threshold. With the 16-by-16 antenna array, even the transmission power is controlled to reach its minimum level, the RA still receives harmful interference at certain altitudes. Note that with 16-by-16 antenna arrays, the peak received interference power is -0.62 dB at the RA height of 116 ft, which is over the threshold of -6 dB. Therefore, h_{zero}, should be set to 121 ft rather than 116 ft, since it is not permitted to deploy 5G base stations within the exclusion zone. It means that the airplanes height should be 138 ft for the exclusion zone rather than 133 ft for the landing safety zone.

TABLE 7. Mean transmission power.

Scenario	Antenna Array	Mean P_t over LSZ (Unit: dBm)	Mean P_t over RZ (Unit: dBm)
Rural	Omnidirectional	45.61	64.23
	4-by-4	45.19	64.16
	8-by-8	39.17	63.19
	16-by-16	33.47	62.39
Suburban	Omnidirectional	45.63	61.07
	4-by-4	44.79	60.96
	8-by-8	39.17	59.88
	16-by-16	33.15	59.18
Urban	Omnidirectional	52.45	62.45
	4-by-4	52	62.28
	8-by-8	45.99	60.84
	16-by-16	39.97	59.83

The mean transmission power, when the airplane is positioned over the landing safety zone and restriction zone, is presented in Table 7. In the suburban scenario, when the airplane hovers over the landing safety zone, the mean transmitted power is 45.63 dBm with the omnidirectional antenna, and 44.79 dBm, 39.17 dBm and 33.15 dBm with 4-by-4, 8-by-8, and 16-by-16 antenna arrays, respectively. Similarly, in the urban scenario, the mean transmitted power is shown as 52.45 dBm for omnidirectional antennas, 52 dBm for 4-by-4, 45.99 dBm for 8-by-8, and 39.97 dBm for 16-by-16 antenna arrays. In the rural environment, the mean reduced transmitted power levels are measured as 45.61 dBm, 45.19 dBm, and 39.17 dBm for the omnidirectional antenna, 4-by-4, and 8-by-8 antenna arrays, respectively. With 16-by-16 antenna arrays, the mean transmitted power is 33.47 dBm considering the landing safety zone.

V. MONTE CARLO SIMULATIONS

In this section, the interference analysis results in Sections III and IV is comprehensively verified. Four cases are assumed

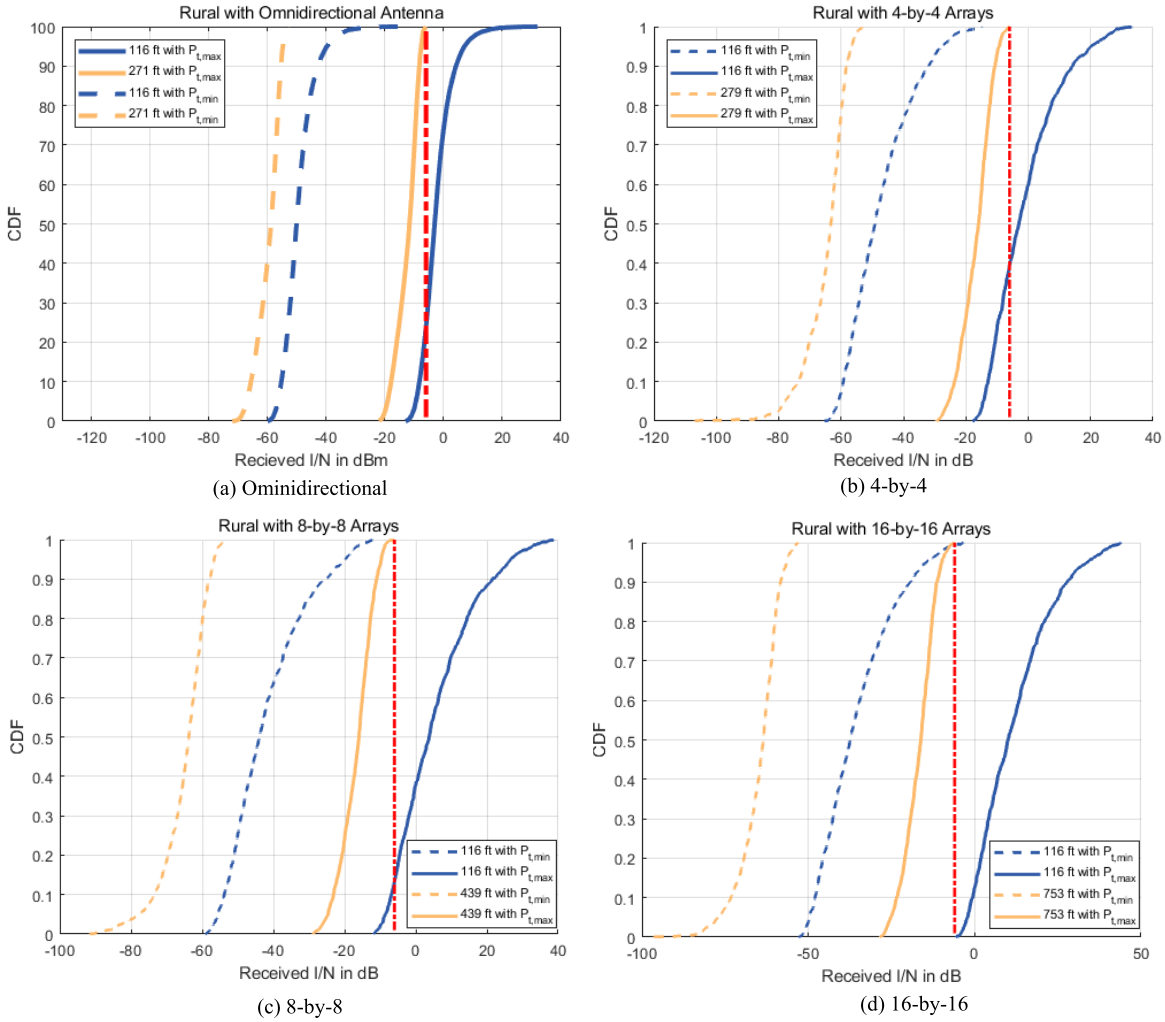

(a) Ominidirectional (b) 4-by-4 (c) 8-by-8 (d) 16-by-16

FIGURE 13. The CDF of Interference-to-noise ratio in the rural scenario with multiple antenna types.

as follows. Case 1 assumes that the airplane is at the edge of the zero-interference zone (h_{zero}) and the 5G base station transmits the maximum transmitted power. Case 2 assumes that the airplane also hovers at h_{zero} but the 5G base station transmits the minimum transmitted power. For Case 3, the airplane is assumed to be at the boundary of the restriction zone (h_{RZ}) and the 5G base station transmits the maximum transmitted power. Finally, the airplane remains at h_{RZ} and the 5G base station transmits the minimum transmitted power in Case 4.

The primary objective of this verification process is to assess the consistency and accuracy of the earlier findings regarding interference analysis while considering the uncertainties and variations inherent in real-world deployment scenarios. For instance, the 5G base station may not be located directly below the RA and the number of UEs can be changed. Therefore, the Monte Carlo method is employed to incorporate random interference phenomena for the simulation. Several parameters such as the random base station location, antenna pointing angle, beamforming direction, channel condition and the random number of UEs are considered. The random base station location is a key factor in determining the arbitrary values of the RA gain and path loss. Additionally, the random direction of the antenna and beamforming play a crucial role in determining the gain of the 5G base station. By incorporating randomness in these parameters, we could effectively model the varying signal strengths and interference levels at the RA. Using the Monte Carlo method, 1,000 snapshots of the RA are generated at the same height within the same environment with the same antenna array. The experimental results are presented in terms of the cumulative distribution function (CDF) to easily compare with the threshold of the RA.

A. RURAL SCENARIO

In the rural scenario, Figure 13 illustrates the simulation performance results with different antenna configurations, namely the omnidirectional antenna, 4-by-4, 8-by-8, and 16-by-16 antenna arrays. The figure features two kinds of curves: solid lines and dotted lines. The solid line corresponds to the case of the 5G base station transmitting the maximum power. meanwhile, the dotted line represents the minimum

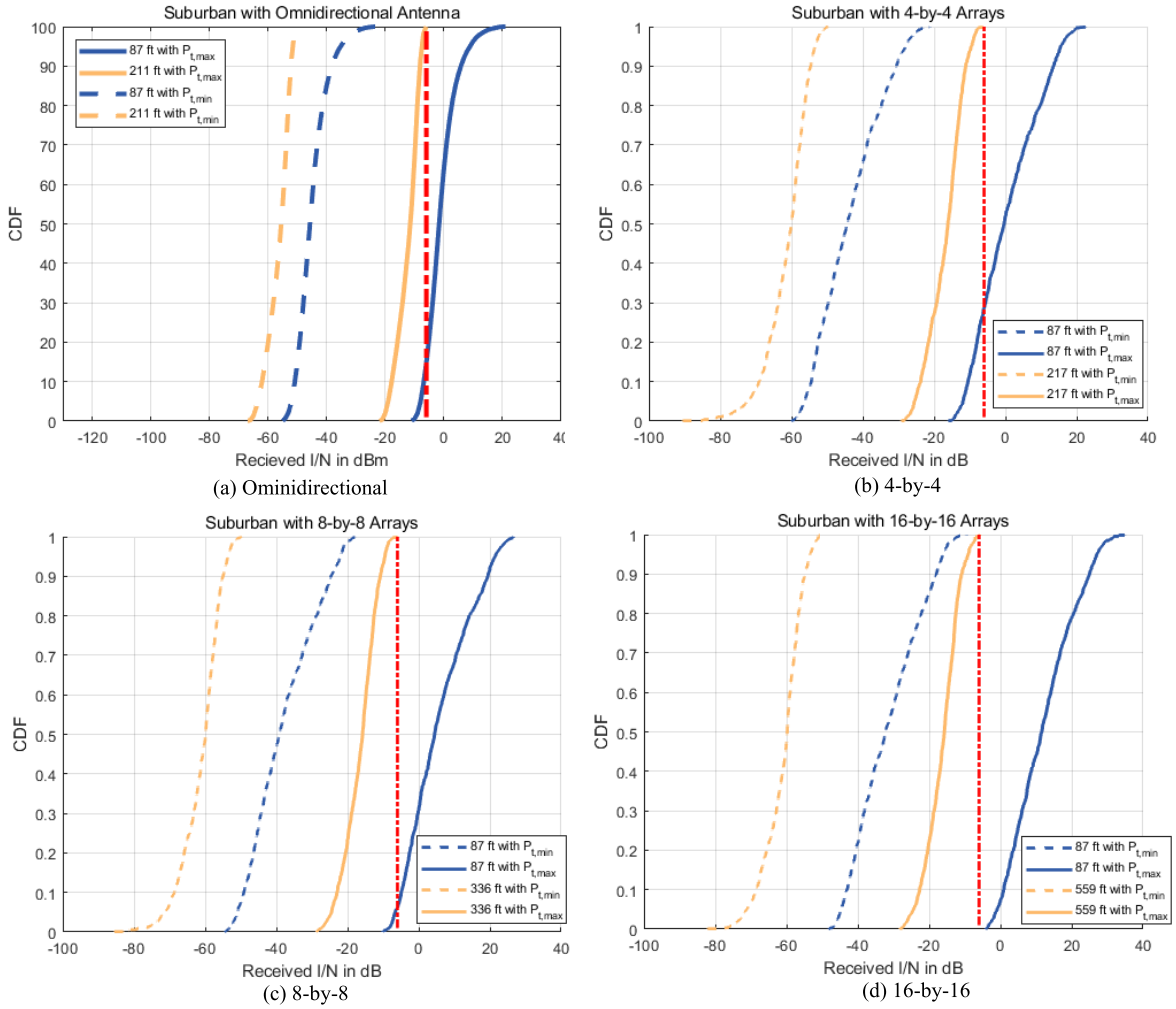

FIGURE 14. Interference-to-noise ratio CDF for the suburban scenario under multiple antenna types.

transmitted power case. Additionally, the blue line represents the case the airplane hovers at h_{zero}, while the orange line depicts the case when the airplane is at h_{RZ}. Note that the simulation results are compared with the protection threshold, i.e., -6 dB, indicated by the red dash-dotted line. The threshold serves as a reference point which can be used as the interference limit.

In the Figure 13, the interference signal power received by the RA surpasses the threshold. Specifically, for the omnidirectional antenna, 4-by-4, 8-by-8, and 16-by-16 antenna arrays, the probability of the received interference power exceeds the interference protection threshold would be 76.34%, 56.5%, 87.7%, and 99.9%, respectively. It is shown that the omnidirectional antenna exhibits a significantly higher probability of exceeding the threshold compared to the 4-by-4 antenna array. Comparing with the omnidirectional antenna lacking a specific directivity, the 4-by-4 antenna array exhibits a more focused and directional radiation pattern, resulting in lower interference levels and a reduced probability of exceeding the threshold.

Generally, the interference signal power received by the RA meets the interference protection threshold, except the 16-by-16 antenna array with the airplane at h_{zero} in Figure 13 (d). In this case, the maximum received interference power reaches -3 dB, which aligns with the interference analysis in Figure 12 (c) in Section IV. Meanwhile, the maximum received interference signal power is around -15 dB, -15 dB, and -12 dB for the omnidirectional antenna, 4-by-4, and 8-by-8 antenna arrays, respectively. It means that it is not necessary to strictly restrict the base station transmit power to the minimum value.

B. SUBURBAN SCENARIO

Figure 14 shows the received interference-to-noise ratio versus different antenna configurations for each base station and the height of the RA in the suburban scenario. It is demonstrated from these figures that in Case 1, the peak received interference is measured at 21 dB, 22 dB, 27 dB, and 34 dB for the omnidirectional antenna, 4-by-4, 8-by-8, and 16-by-16 antenna arrays, respectively. Note that these peak values closely resemble the peak values observed in the suburban

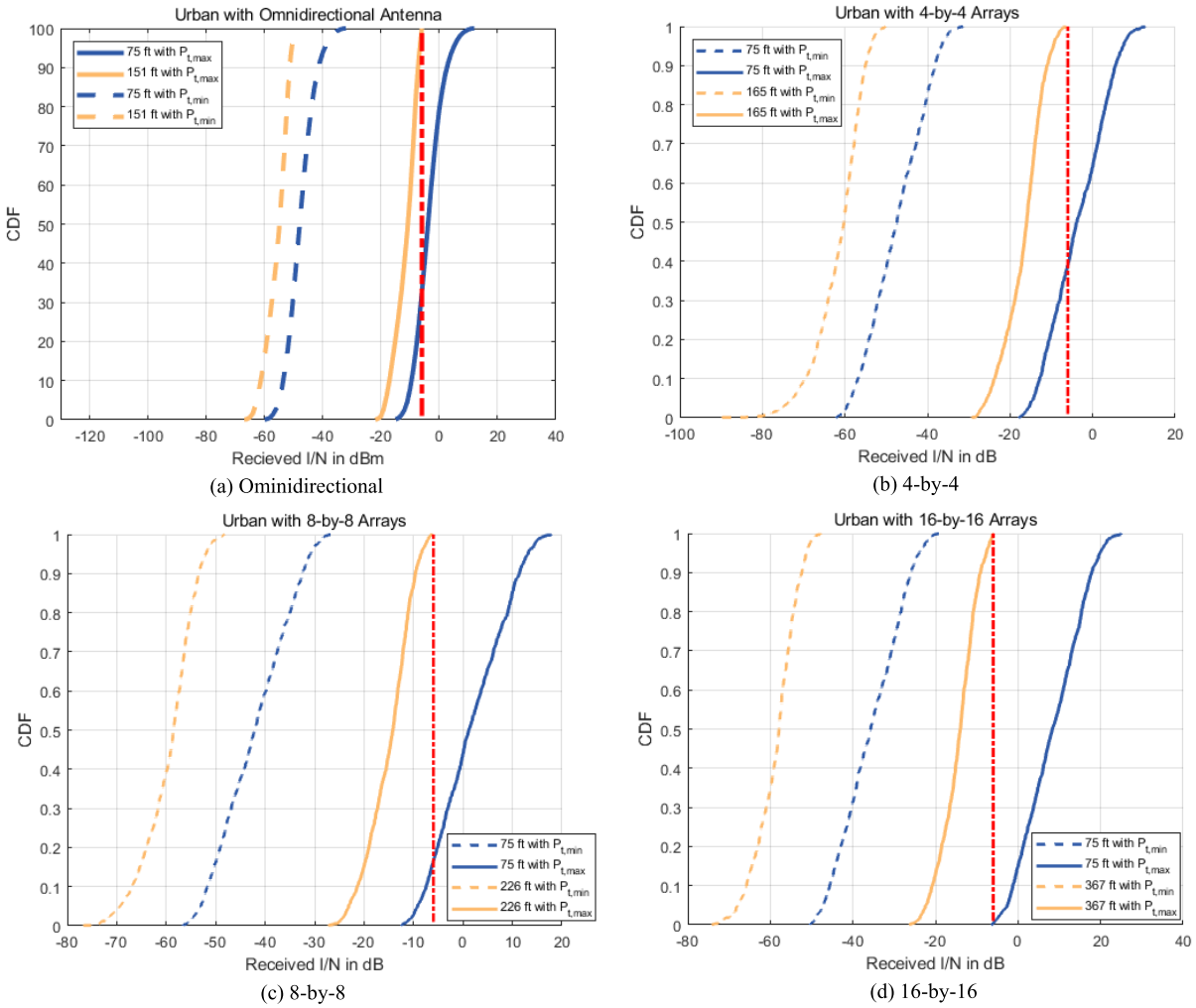

(a) Ominidirectional (b) 4-by-4 (c) 8-by-8 (d) 16-by-16

FIGURE 15. Interference-to-noise ratio CDF for the urban scenario under multiple antenna types.

scenario in Figure 10 (b) in Section III. For the omnidirectional antenna, 4-by-4, 8-by-8, and 16-by-16 antenna arrays, the percentages of received interference power exceeding the protection threshold is 85.37%, 69.7%, 92.5%, and 100%, respectively. In Case 2, the maximum interference received by RA is approximately -21 dB, -21 dB, -17 dB, and -9 dB for the omnidirectional, 4-by-4, 8-by-8, and 16-by-16 antenna arrays, respectively. This suggests that it may not be necessary to limit the 5G base station transmitted power to the minimum value because of the gap with the threshold. In Case 3, the maximum interference received by RA remains constant -6 dB with all antenna configurations, aligning with Figure 10 (b) in Section III.

C. URBAN SCENARIO

The percentage of received interference power surpassing the protection threshold follows a similar trend in the urban area, in a similar way to the rural and suburban areas. The specific percentages of received interference power exceeding the protection threshold for each antenna configuration is 67.46% for the omnidirectional antenna, 58.5% for the 4-by-4 array, 81.5% for the 8-by-8 array, and 99.1% for the 16-by-16 array, respectively. These results indicate that the omnidirectional antenna has a higher probability of experiencing interference beyond the established protection threshold compared to the 4-by-4 antenna array. As the number of antenna elements increases, the probability of exceeding the protection threshold also tends to rise. In Case 1, the maximum received interference power is 11 dB, 12 dB, 18 dB, and 21 dB for the omnidirectional antenna, 4-by-4, 8-by-8, and 16-by-16 antenna arrays, respectively. Note that the maximum received interference remains -6 dB for all antenna configurations for Case 3 corresponding to the Figure 10 (c) in Section III. In Case 2, the received interference with the omnidirectional antenna, the 4-by-4, 8-by-8, and 16-by-16 antenna arrays is far below the threshold, when the maximum received interference is -31 dB, -31 dB, -26 dB, and -19 dB, respectively. It is found that with various antenna configurations, the maximum received interference in the urban scenario is the lowest and the highest in the rural scenario. This tendency is well matched with Figure 10 in Section III.

VI. CONCLUSION

This paper proposed a mathematical method for interference analysis to investigate the potential coexistence of 5G base stations with existing RAs operating in the 4.2–4.4 GHz band. For accurate analysis, the airplane route was divided into the landing safety zone and zero-interference zone, considering aircraft safety precautions for departure and arrival. The interference was analyzed for the worst-case scenario with various losses, so that the scope of receiving harmful interference from 5G base stations is obtained.

The simulation results were shown in comparison to the interference protection threshold of the RA. It was found that when the protection threshold was reached, the different altitudes were achieved in the rural, suburban, and urban scenarios. Furthermore, a distance-based power control scheme was introduced to mitigate the interference and realize the coexistence of 5G communication systems with RAs. Additionally, the exclusion and the restriction zones were introduced to enable the coexistence between the RA and the 5G base stations. Furthermore, the Monte Carlo method was employed to validate the effectiveness of the proposed protection method. The Monte Carlo results are well matched with the static simulation results for the worst case. The results for the interference analysis without and with the protection method may be a useful reference for the researchers.

For future work, it is necessary to test the projected models using practical measured data. Furthermore, more mitigation techniques are under considered, such as restricting the pointing angles of the 5G base station antennas, lowering the height of 5G base stations, and minimizing interference by designing highly effective filters.

REFERENCES

[1] T. Miller, S. Wongsaroj, V. Jervis, and R. Rudd. (2023). *Examining the Current Assignment and Usage of Mobile Spectrum*. Accessed: Jan. 12, 2024. [Online]. Available: https://www.apt.int/sites/default/files/Examining_the_current_assignment_and_usage_of_mobile_spectrum.pdf

[2] Mid-Band Spectrum and The Coexistence with Radio Altimeters, 5G Americas White Paper. (Jul. 2020). Accessed: Jan. 17, 2024. [Online]. Available: https://5gamericas.org/wp-content/uploads/2021/07/Mid-Band-Spectrum-and-the-Co-Existence-with-Radio-Altimeters.pdf

[3] D. Shepardson. (2021). *US Warns 5G Wireless Use Could Prompt Flight Diversions*. Accessed: Jan. 17, 2024. [Online]. Available: https://www.reuters.com/business/aerospace-defense/us-warns-5g-wireless-use-could-prompt-flight-diversions-2021-12-07/

[4] G. Wallace, P. Muntean, and M. Ballaban. (Jan. 19, 2022). *International Airlines Suspend Some US Flights Over 5G Uncertainty*. Accessed: Jan. 17, 2024. [Online]. Available: https://edition.cnn.com/2022/01/18/business/airline-cancellations-5g/index.html

[5] *Operational and Technical Characteristics and Protection Criteria of Radio Altimeters Utilizing the Band 4200–4400 MHz*, document ITU-R M.2059-0, 2024. [Online]. Available: https://www.itu.int/dms_pubrec/itu-r/rec/m/R-REC-M.2059-0-201402-I!!PDF-E.pdf

[6] (Jun. 29, 2023). *Aircraft Operations and Radar Altimeter Interference From 5G, Air Line Pilots Association (ALPA)*. Accessed: Jan. 12, 2024. [Online]. Available: https://www.alpa.org/resources/aircraft-operations-radar-altimeter-interference-5G

[7] M-H Cho. (2020). *South Korea To Reallocate Mid-Band Spectrum for 5G Use*. Accessed: Jan. 17, 2024. [Online]. Available: https://www.zdnet.com/article/south-korea-to-reallocate-spectrum-for-5g-use/

[8] Y. Cho, H.-K. Kim, M. Nekovee, and H.-S. Jo, "Coexistence of 5G with satellite services in the millimeter-wave band," *IEEE Access*, vol. 8, pp. 163618–163636, 2020, doi: 10.1109/ACCESS.2020.3022044.

[9] E. Lagunas, C. G. Tsinos, S. K. Sharma, and S. Chatzinotas, "5G cellular and fixed satellite service spectrum coexistence in C-band," *IEEE Access*, vol. 8, pp. 72078–72094, 2020, doi: 10.1109/ACCESS.2020.2985012.

[10] Y. Wei, S. Liu, and S.-H. Hwang, "Distance protection for coexistence of 5G base station and satellite earth station," *Electronics*, vol. 10, p. 1481, Jun. 2021, doi: 10.3390/electronics10121481.

[11] R. Singh, R. Peterson, A. Riaz, C. Hood, R. Bacchus, and D. Roberson, "A method for evaluating coexistence of LTE and radar altimeters in the 4.2–4.4 GHz band," in *Proc. Wireless Telecommun. Symp. (WTS)*, Apr. 2017, pp. 1–9, doi: 10.1109/WTS.2017.7943543.

[12] (Oct. 7, 2073). *Assessment of C-Band Mobile Telecommunications Interference Impact on Low Range Radar Altimeter Operations*. Accessed: Jan. 17, 2024. [Online]. Available: https://www.rtca.org/wp-content/uploads/2020/10/SC-239-5G-Interference-Assessment-Report_274-20-PMC-2073_accepted_changes.pdf

[13] H. K. Son and Y.-J. Chong, "Interference analysis for compatibility between 5G system and aeronautical radio altimeter," in *Proc. Int. Conf. Inf. Commun. Technol. Converg. (ICTC)*, 2020, pp. 1553–1556, doi: 10.1109/ICTC49870.2020.9289432.

[14] S. Futatsumori, N. Miyazaki, A. Sato, R. Ozaki, T. Hikage, and T. Nojima, "Measurement of 4 GHz radio altimeter interference path loss including 5G sub-6 frequency bands using beechcraft B300 aircraft," in *Proc. Int. Symp. Antennas Propag. (ISAP)*, Oct. 2021, pp. 1–2, doi: 10.23919/ISAP47258.2021.9614476.

[15] S. Futatsumori, N. Miyazaki, N. Hiraga, K. Kobayashi, and K. Nakafukushima, "Helicopter radio altimeter interference path loss measurement including adjacent 5G mobile telecommunications band," in *Proc. IEEE Asia–Pacific Microw. Conf. (APMC)*, Nov. 2021, pp. 476–478, doi: 10.1109/APMC52720.2021.9662023.

[16] S. Futatsumori and N. Miyazaki, "Evaluation of pulsed aircraft radio altimeter electromagnetic interference characteristics due to sub-6 band 5G mobile communication systems," *Inst. Electron., Inf. Commun. Eng. (IEICE) Tech. Rep.*, vol. 121, pp. 139–143, Nov. 2021.

[17] I. Bor-Yaliniz, M. Salem, G. Senerath, and H. Yanikomeroglu, "Is 5G ready for drones: A look into contemporary and prospective wireless networks from a standardization perspective," *IEEE Wireless Commun.*, vol. 26, no. 1, pp. 18–27, Feb. 2019, doi: 10.1109/MWC.2018.1800229.

[18] S. Homayouni, M. Paier, C. Benischek, G. Pernjak, M. Leinwather, M. Reichelt, and C. Fuchsjager, "On the feasibility of cellular-connected drones in existing 4G/5G networks: Field trials," in *Proc. IEEE 4th 5G World Forum (5GWF)*, Montreal, QC, Canada, Oct. 2021, pp. 287–292, doi: 10.1109/5GWF52925.2021.00057.

[19] A. Fakhreddine, C. Bettstetter, S. Hayat, R. Muzaffar, and D. Emini, "Handover challenges for cellular-connected drones," in *Proc. 5th Workshop Micro Aerial Vehicle Netw., Syst., Appl.*, Jun. 2019, pp. 9–14, doi: 10.1145/3325421.3329770.

[20] N. Sehad, X. Tu, A. Rajasekaran, H. Hellaoui, R. Jäntti, and M. Debbah, "Towards enabling reliable immersive teleoperation through digital twin: A UAV command and control use case," 2023, *arXiv:2308.14524*.

[21] S. Liu, J. Li, S.-H. Hwang, H.-K. Son, and Y.-J. Chong, "Interference analysis method for 5G system to radio altimeter," in *Proc. IEEE VTS Asia Pacific Wireless Commun. Symp. (APWCS)*, Jun. 2022, pp. 80–84, doi: 10.1109/APWCS55727.2022.9906499.

[22] A. Abbas, M. Elsaid, S. F. Mahmoud, E. A. Abdallah, and H. M. El-Hennawy, "Link budget analysis for FMCW radio altimeter," in *Proc. Int. Telecommun. Conf. (ITC-Egypt)*, Jul. 2021, pp. 1–4, doi: 10.1109/ITC-Egypt52936.2021.9513976.

[23] *Modelling and Simulation of IMT Networks and Systems for Use Sharing and Compatibility Studies*, document ITU-R M.2101-0, 2024. [Online]. Available: https://www.itu.int/dms_pubrec/itu-r/rec/m/R-REC-M.2101-0-201702-I!!PDF-E.pdf

[24] M. Irsigler, G. W. Hein, and A. Schmitz-Peiffer, "Use of C-band frequencies for satellite navigation: Benefits and drawbacks," *GPS Solutions*, vol. 8, no. 3, pp. 119–139, Sep. 2004, doi: 10.1007/s10291-004-0098-2.

[25] A. Roy, "Preliminary study into radio altimeter adjacent band compatibility," in *Proc. 30th Meeting Working F, Aeronautical Commun. Panel (ACP)*, Mar. 2014. [Online]. Available: https://www.icao.int/safety/acp/ACPWGF/ACP-WG-F-30/ACP-WGF30-WP14%20Radio%20Altimeter%20Adjacent%20Bands%20Compatibility%20Study%20with%20IMT-FINAL%20Rev1.docx

[26] *Study on Channel Model for Frequencies From 0.5 To 100 GHz, Release 16*, document TR 38.901 V16.1.0, 3GPP, 2020. [Online]. Available: https://www.etsi.org/deliver/etsi_tr/138900_138999/138901/16.01.00_60/tr_138901v160100p.pdf

[27] (Mar. 31, 2012). *Methods and Tools for Estimating Spectrum Availability: Case of Multiple Secondary Users, Report D5.3 120331, ICT-248303, QUASAR*. Accessed: Jan. 11, 2024. [Online]. Available: https://cordis.europa.eu/docs/projects/cnect/3/248303/080/deliverables/001-QUASARD53.pdf
[28] *Landing Zone Preparation and Safety, in Beacon Health System*. Accessed: Jan. 17, 2024. [Online]. Available: https://www.beaconhealthsystem.org/beacon-medical-transport/landing-zone-preparation-and-safety/
[29] S. Nakamura, K. Suwa, S. Morita, K. Yamamoto, T. Wakayama, T. Oshima, R. Maekawa, and S. Matsuda, "An experimental study of enhancement of the cross-range resolution of ISAR imaging using ISDB-T digital TV based passive bistatic radar," in *Proc. IEEE Int. Geosci. Remote Sens. Symp.*, Jul. 2011, pp. 2837–2840, doi: 10.1109/IGARSS.2011.6049805.
[30] Naver Blog. (May 6, 2021). *Normal Approach and Landing*. Accessed: Jan. 17, 2024. [Online]. Available: https://m.blog.naver.com/easyworldeasylife/222339970028
[31] D. Bear. *Normal Approach and Landing*. ALC-34: Maneuvering: Approach Landing, Federal Aviation Admin. (FAA). Accessed: Jan. 11, 2024. [Online]. Available: https://www.faasafety.gov/files/helpcontent/Courses/ALC-34/content/index.html#/
[32] (Jun. 29, 2021). *Characteristics of Terrestrial Component of IMT For Sharing and Compatibility Studies in Preparation for WRC-23, ITU Annex 4.4 To Working Party 5D Chairman's Report*. [Online]. Available: https://www.itu.int/md/R19-WP5D.AR-C-0318/_page.print
[33] Skybrary. *Landing Distances*. Accessed: Jan. 17, 2024. [Online]. Available: https://www.skybrary.aero/articles/landing-distances
[34] K. Behnke. (Mar. 26, 2019). *'Is This Anything To Worry About? 5G Health Issues Explained*. GrandMetric. Accessed: Jan. 17, 2024. [Online]. Available: https://www.grandmetric.com/2019/03/26/5g-health-issues-explained/
[35] *5G NR Sub-6 GHz Measurement Methods: Signal Analyzer MS2850A, ANRITSU*. Accessed: Jan. 17, 2024. [Online]. Available: https://dl.cdn-anritsu.com/en-en/test-measurement/files/Application-Notes/Application-Note/ms2850a-5gnr-ef1200.pdf
[36] (Feb. 6, 2018). *Radio Altimeter Spectrum, ICAO*. Accessed: Jan. 17, 2024. [Online]. Available: https://www.icao.int/NACC/Documents/Meetings/2018/RPG/RPGITUWRC2019-P08.pdf
[37] M. Finlay. (Jul. 25, 2020). *WestJet Boeing 737 Conducted A Flapless Landing in Deer Lake*. Accessed: Jan. 17, 2024. [Online]. Available: https://simpleflying.com/westjet-737-flapless-landing/
[38] *Propagation Data and Prediction Methods for the Planning of Short-Range Outdoor Radiocommunication Systems and Radio Local Area Networks in the Frequency Range 300 MHz To 100 GHz*, document ITU-R P.1441-2, 2024. [Online]. Available: https://www.itu.int/dms_pubrec/itu-r/rec/p/R-REC-P.1411-2-200304-S!!MSW-E.doc

JIAQI LI (Member, IEEE) received the B.S. degree in communication engineering from the North China University of Science and Technology, Tangshan, China, in 2016, and the M.Sc. degree (Hons.) in communications and signal processing from the University of Leeds, Leeds, U.K., in 2021. She is currently pursuing the Ph.D. degree with the Department of Electronics and Electrical Engineering, Dongguk University, Seoul, South Korea. From 2016 to 2020, she was a Lecturer for experimental courses related to MATLAB, digital signal processing, and engineering drawing with the Department of Information Science, Xinhua College of Sun Yat-sen University, Guangzhou, China. Her research interests include 5G/6G technologies, cloud-fog architecture, the Internet of Things (IoT), and energy efficiency of distributed networks focusing on the use of renewable energy. She was recipient of the Conference Best Paper Award from IEEE VTS APWCS, in 2022.

SHUZHI LIU (Graduate Student Member, IEEE) received the B.S. degree in mechanical engineering from Hanyang University, Ansan, South Korea, in 2018. He is currently pursuing the integrated master's and Ph.D. degree with the Department of Electronics and Electrical Engineering, Dongguk University, Seoul, South Korea. His research interests include 5G/6G spectrum technologies, the Internet of Things (IoT), and high precision indoor positioning. He was a recipient of two conference best paper awards from IEEE VTS APWCS, in 2019 and 2022.

HOUJIN LU (Graduate Student Member, IEEE) received the B.S. degree in electrical engineering and automation from Ningbo University of Technology, Ningbo, China. He is currently pursuing the integrated master's and Ph.D. degree with the Department of Electronics and Electrical Engineering, Dongguk University, Seoul, South Korea. His main research interests include 5G mobile networks and wireless communication systems.

SEUNG-HOON HWANG (Senior Member, IEEE) received the Ph.D. degree in electrical engineering from Yonsei University, Seoul, Republic of Korea, in 1999. From 1999 to 2004, he worked for UMTS standardization with LG Electronics, Republic of Korea. From 2003 to 2004, he was a Visiting Research Fellow with the University of Southampton, U.K., with Prof. Lajos Hanzo. In 2010, he was a Visiting Professor with Stanford University, Stanford, CA, USA, with Prof. John Cioffi. He is currently a Professor with the Division of Electronics and Electrical Engineering and the Dean of the Engineering School, Dongguk University, Seoul. He received awards from the Minister of Education and the Minister of Science and ICT, respectively. He was a recipient of the British Chevening Scholarship funded by the Foreign and Commonwealth Office, U.K. He is the Chairperson of the IEEE VTS Seoul Chapter, the Vice President of the Korean Institute of Communications and Information Sciences, South Korea, and the Chairperson of the Spectrum Committee in the 6G Forum, South Korea.